Core Losses and Torque Ripple in IPM Machines: Dedicated Modeling and Design Trade Off

Core Losses and Torque Ripple in IPM Machines: Dedicated Modeling and Design Tradeoff

Gianmario Pellegrino, *Member, IEEE*, Paolo Guglielmi, *Member, IEEE*, Alfredo Vagati, *Fellow, IEEE*, and Franco Villata

***Abstract*—The proper combination of stator and rotor slot numbers is pursued in the design of interior permanent-magnet (IPM) motors with wide constant-power speed range. At high speed, in the flux-weakening region, the arising of stator and rotor iron losses due to magnetomotive-force (MMF) spatial harmonics limits the IPM motor performance. Torque ripple is another problem for this kind of machines, both at low and high speed. The numbers of stator slots and rotor equivalent slots have a major impact on both the loss and ripple aspects. A simplified model is proposed here in order to evaluate both problems with a general approach and point out the possible design tradeoff. With respect to previous models in the literature, both stator and rotor losses are included, and a more comprehensive approach is followed in the description of the rotor MMF harmonics. The model's effectiveness is tested through finite element analysis simulations and some experimental results. The proposed approach is useful for the selection of the IPM machine structure according to the specific requirements of the application.**

***Index Terms*—Permanent-magnet motors, synchronous motor drives.**

I. Introduction

THE USE of interior permanent-magnet (IPM) motors in many different applications is growing constantly. In particular, these motors are appreciated for their good efficiency and large speed ranges due to their field-weakening capability, provided that the motor is suitably designed for that aim. However, at high speed, the performance of the IPM motors can be seriously limited by iron losses. As the speed increases, the machine flux is lowered, but the harmonic fields do not reduce accordingly. At high frequency, the eddy currents generated by the harmonic fields become significant both in the stator and in the rotor cores, and the motor performance is limited both at load and at no load conditions since a demagnetizing current can be required at high speed also at no load. As a consequence, the prediction of such harmonic losses is of great importance to address the motor design to loss minimization. Torque ripple is also a problem for this kind of machines. With poor design choices, it can become significant and lead to vibrations at any speed. Both torque ripple and core losses are in strong relationship with the choice of the stator and rotor "slot" numbers. The concept of rotor slot number $\mathrm{n_r}$ has been introduced in ripple and loss modeling in [4], [10] and [7], [9], respectively. It relies on equally divided rotor teeth along the air-gap surface. This is one of the hypotheses of this paper.

The torque ripple modeling and its relationship with the slot combinations has been first proposed for synchronous reluctance motors [4]. More recently, such analysis has been extended to IPM motors [10]. Dealing with high speed losses, the subject has been present in the literature since 1989 [1]. It has been recently shown in [7], [9] that the stator and rotor slot harmonics can have a dominant impact on these losses. Other kinds of losses, e.g., those in the permanent magnets, have been shown to be less important, at least if motors with fractional slots per pole per phase are not considered.

Proper combinations of stator and rotor slots per pole pair (n_s and n_r) help minimize torque ripple, while other combinations minimize high speed losses. This paper confirms that the optimal combinations for torque ripple and core losses are, in general, different and that the IPM motor design must be a tradeoff between the two needs. An example of such a tradeoff is given by [7], where some specific design choices are considered and evaluated.

In this paper, a generalized approach to this design tradeoff is presented based on a simplified modeling of both torque ripple and core losses mechanisms. The obtained results allow a synthetic overview of the problem, leading to comparable quantitative results for different n_s, n_r combinations. In addition, this modeling represents a tool that is capable of addressing the basic design choices (rotor bore, air-gap flux density, ...) without necessarily requiring a large number of finite element analysis (FEA) simulations. Of course, the final design step will necessarily refer to a FEA evaluation if a reliable prediction of the motor performance is wanted. The FEA simulations are used for confirming the results of the proposed analysis. The torque ripple is also evaluated experimentally and compared with FEA results.

II. Torque Ripple and Eddy-Current Loss Modeling

This section derives the analytical expression for the IPM torque ripple and eddy-current losses under the idealized assumptions of no magnetic saturation and closed stator slots.

Most of the analytical part is dedicated to the description of the magnetomotive-force (MMF) staircase spatial functions and

Manuscript received October 12, 2009; revised February 15, 2010; accepted March 29, 2010. Date of publication September 2, 2010; date of current version November 19, 2010. Paper 2009-EMC-339.R1, presented at the 2009 IEEE Energy Conversion Congress and Exposition, San Jose, CA, September 20–24, and approved for publication in the IEEE Transactions on Industry Applications by the Electric Machines Committee of the IEEE Industry Applications Society.

The authors are with the Politecnico di Torino, 10129 Torino, Italy (e-mail: gianmario.pellegrino@polito.it; paolo.guglielmi@polito.it; alfredo.vagati@polito.it; franco.villata@polito.it).

Color versions of one or more of the figures in this paper are available online at http://ieeexplore.ieee.org.

Digital Object Identifier 10.1109/TIA.2010.2072971

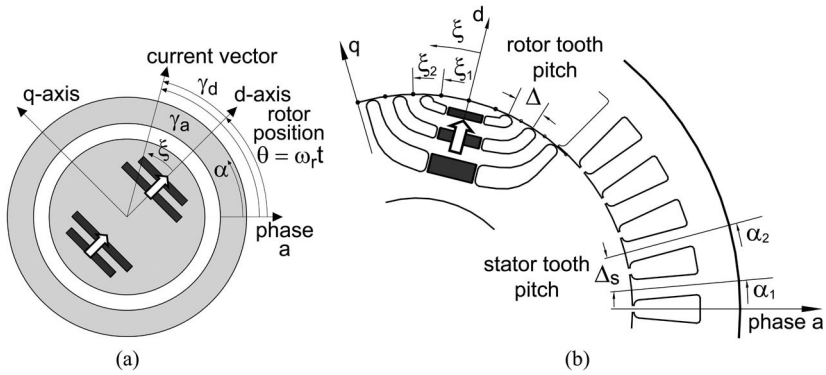

Fig. 1. (a) Definition of the reference frames on a 2-pole machine. (b) Stator and rotor slot pitch definition.

the relationship between the MMF harmonic content and the stator and rotor slot numbers. With respect to the most recent expression available in the literature [10], the analysis presented also deals with the contribution to torque ripple given by the pulsating rotor harmonics that are produced as a reaction to stator MMF harmonics other than the fundamental one.

The assumed reference frames are shown in Fig. 1, where $\theta = \omega_r \cdot t$ is the rotor angle, as measured from the d-axis (aligned to the PM flux) to the stationary reference, as taken from the phase a axis. α and ξ are the stator and rotor angular coordinates, respectively.

A. Stator MMF

The winding function N is given in (1). If the three phase windings are connected in a floating star configuration, the stator MMF $f_s\ (\alpha, \theta)$ can be written by (2) and (3), where the rotor angle $\theta = \omega_r \cdot t$ has been introduced

$$N = \sum_{h=1,2,3,\ldots} \hat{n}_h \cdot \cos(h\alpha) \tag{1}$$

$$f_s = \sum_{h=1,4,7,\ldots} 1.5 \cdot \hat{n}_h i_m \cdot \cos(h\alpha - \gamma_a) + \sum_{h=2,5,8,\ldots} 1.5 \cdot \hat{n}_h i_m \cdot \cos(h\alpha + \gamma_a) \tag{2}$$

$$f_s = \sum_{h\neq 3,6,9,\ldots} \hat{f}_{sh} \cdot \cos(h\alpha \mp \omega_r t \mp \gamma_d). \tag{3}$$

B. Rotor Sampling of the hth Stator MMF

The rotor MMF can be written by the general form (4), where the presence of cosinusoidal terms only stands for the existing symmetry with respect to the d-axis [10]

$$f_r = \sum_{k\neq 2,4,6,\ldots} \hat{f}_{rk} \cdot \cos(k\xi). \tag{4}$$

In the following, the part of (4) that is generated as a reaction of the flux barriers in the IPM rotor to the stator MMF (3) will be considered, and the relationship between stator and rotor MMF distributions will be expressed analytically. The rotor magnetic potentials due to the permanent magnets and the flux-flow through the rotor barriers and through the thin iron ribs will be disregarded at this point.

With respect to previous works, [10] it will be shown that some of the f_r harmonics in (4) have an amplitude that varies with the rotor position θ and consequently with time, despite all the stator harmonics in (3), have a constant amplitude. This is the effect of the rotor anisotropy over those stator harmonic fields that are not synchronous to the rotor: the resulting rotor fields are modulated by the rotor position. The stator fundamental component, $h = 1$ in (3), is synchronous to the rotor and will produce rotor orders with constant amplitude like in [10], while higher stator orders $(h > 1)$ are not synchronous to the rotor, and will produce rotor orders with a variable amplitude.

It is assumed that the rotor cavities are equally spaced along the air-gap surface in order to define a rotor slot number n_r and a corresponding rotor pitch Δ. In order to evaluate the relationship between stator MMF (3) and rotor reaction MMF in the following, each hth harmonic component of the stator MMF will be separately considered as the input signal of a digital sampling process. The hth stator harmonic is expressed as a function of the rotor coordinate $\xi = \alpha + \omega_r t$ and the current phase angle $\gamma_{\rm d} = \gamma_{\rm a} - \omega_r t$ in

$$f_{sh} = \hat{f}_{sh} \cdot \cos\left[h\xi + (h \mp 1) \cdot \omega_r t \mp \gamma_d\right] = \hat{f}_{sh} \cdot \cos[h\xi + \varphi] \tag{5}$$

where $\varphi = (h \mp 1) \cdot \omega_r t \mp \gamma_d$ has been introduced for more compactness. As shown in Fig. 2, the stator harmonic f_{sh} is averaged by the rotor teeth, thus leading to a staircase waveform. The step levels c_{hj} shown in Fig. 2 are obtained as the average of f_{sh} over one rotor pitch

$$c_{hj} = \frac{1}{\Delta} \int_{\xi_j}^{\xi_{j+1}} \cos(h\xi + \varphi) \cdot d\xi \tag{6}$$

where h stands for the stator harmonic order and j stands for the jth rotor tooth.

The c_{hj} levels are a function of the rotor position according to the term φ in (6). The analytical model of a discrete-time sampling process is adopted here [11], where the angular coordinate ξ is used instead of time, the rotor angular pitch Δ corresponds to the sample time T, and the rotor slot number $n_r = 2\pi/\Delta$ corresponds to the sample pulsation $\omega_s = 2\pi/T$. The transfer function between the sinusoidal input signal f_{sh} and the output staircase function indicated as f_{rs} (effect of

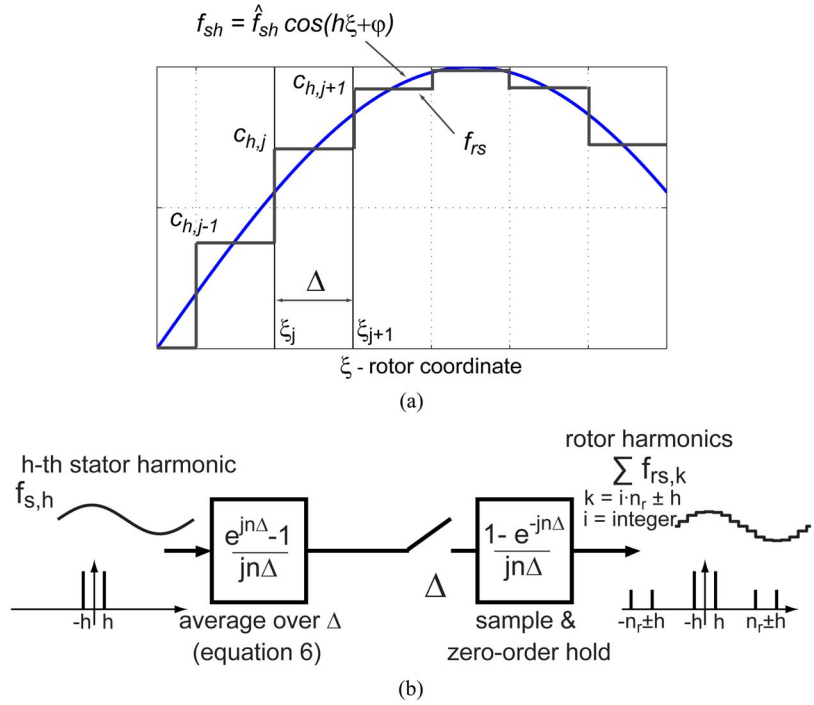

Fig. 2. Averaging effect of the rotor teeth of a multilayer rotor over the hth order stator harmonic $f_{sh}\cos(h\xi+\varphi)$. (a) Staircase function obtained by averaging the sinusoidal MMF along the rotor teeth. (b) Transfer function of the staircase generation process.

the stator MMF on the rotor) is expressed in terms of Fourier transform blocks in Fig. 2(b). The usual delay transfer function e^{-sT} is written as $e^{-jn\Delta}$ since the Laplace variable s equals jn for the generic nth order harmonic. From left to right in Fig. 2(b), the input sinusoidal function f_{sh} is first integrated ($1/jn\Delta$ term), then the integrated value is anticipated by Δ ($e^{jn\Delta}$ term) and the difference is taken between the anticipated and the current value of the integral ($e^{jn\Delta}-1$ term at the numerator). The output of the transfer function at the left side of Fig. 2(b) is the moving average of f_{sh} over one rotor pitch. The moving average is sampled at the rotor cavity angles ξ_j ($j = 1 \div n_r$) shown in Figs. 1(b) and 2(a) and the c_{hj} values (6) are obtained. Furthermore, the zero-order-hold transfer function is introduced to hold the c_{hj} samples along one rotor pitch.

Both the transfer functions in Fig. 2(b) have the same amplitude, while their arguments have opposite signs as shown by (7) and (8), respectively,

$$\frac{e^{j\Delta n}-1}{j\Delta n} = \frac{\sin(n\Delta/2)}{n\Delta/2}\cdot e^{j(n\Delta/2)} \tag{7}$$

$$\frac{1-e^{-j\Delta n}}{j\Delta n} = \frac{\sin(n\Delta/2)}{n\Delta/2}\cdot e^{-j(n\Delta/2).} \tag{8}$$

The function $\sin c(n\pi/n_r) = \sin(n\pi/n_r)/(n\pi/n_r)$ is shown in Fig. 3, where $\Delta = 2\pi/n_r$ has been substituted in (7) and (8) and n represents the generic harmonic order. Since the inputs are sinusoidal functions, the spectra are symmetric with respect to n and are plotted here for $n > 0$ only.

As shown in Fig. 3, each hth harmonic produces infinite kth harmonics on the rotor due to the sampling process; in particular, h reproduces itself plus the sidebands around the multiples of n_r. The output (rotor) orders are $k = i \cdot n_r \pm h$, where the index i is any integer. With reference to the hth stator

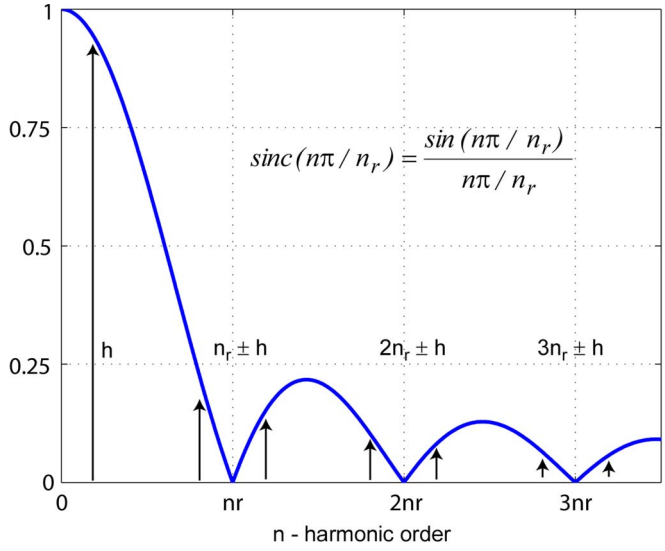

Fig. 3. sinc( ) function in the axis of slot numbers n.

harmonic (5), the output of the sampling process of Fig. 2(b) is expressed by

$$\frac{f_{rs,k}}{\hat{f}_{sh}} = (-1)^i \cdot \sin c\left(\frac{h\pi}{n_r}\right)\sin c\left(\frac{k\pi}{n_r}\right)\cos(k\xi+\varphi) \qquad k \neq \frac{n_r}{2}, \frac{3n_r}{2}, \ldots \tag{9}$$

with $k = i \cdot n_r \pm h$. Regarding the amplitude of (9), consider that tsecond, to the kth harmonic by the zero-order hold. Dealing with phase angles, the arguments of (7) and (8) are $h\Delta/2$ and $-k\Delta/2$, respectively, which correspond to $h\pi/n_r$ and $-k\pi/n_r$. Thus, the overall phase shift angle is $(h-k)\cdot \pi/n_r = i\pi$, which is represented by the factor $(-1)^i$ in (9).

Moreover, it can be shown that the output of (9) is zero for those stator orders, which are odd multiples of $n_r/2 (h = n_r/2, 3/2 \cdot n_r, \ldots)$. In this cases, the spectral lines obtained in Fig. 3 are coupled two by two (e.g., h with $n_r - h$, $n_r + h$, and $2n_r + h \ldots$) and out of phase due to $(-1)^i$. As a consequence, they cancel each other out. The term f_{rs} in (9) does not represent the rotor reaction MMF yet, as explained in the following.

C. Rotor MMF

The MMF staircase f_{rs}, whose kth term is expressed in (9), can be split into the two components defined in (10), which are symmetric with respect to the d-axis and the q-axis, respectively,

$$f_{rs+} = \frac{f_{rs}(\xi) + f_{rs}(-\xi)}{2}$$
$$f_{rs-} = \frac{f_{rs}(\xi) - f_{rs}(-\xi)}{2}. \tag{10}$$

The former term (11) represents the rotor reaction to the stator MMF and thus, it is a component of the rotor MMF, while (12) is short-circuited by the rotor iron channels and produces flux circulation and related losses in the rotor channels

$$f_{rs+,k} = (-1)^i \cdot \hat{f}_{sh} \cdot \sin c(h\pi/n_r) \sin c(k\pi/n_r) \cdot \cos\left[(h \mp 1) \cdot \omega_r t \mp \gamma_d\right] \cdot \cos(k\xi) \tag{11}$$
$$f_{rs-,k} = (-1)^i \cdot \hat{f}_{sh} \cdot \sin c(h\pi/n_r) \sin c(k\pi/n_r) \cdot \sin\left[(h \mp 1) \cdot \omega_r t \mp \gamma_d\right] \cdot \sin(k\xi) \tag{12}$$

where $k = i \cdot n_r \pm h$, $h \neq (2l+1) \cdot n_r/2$, and l and i are integers.

Apart from f_{rs+}, the other terms that contribute to the rotor MMF are the MMF due to the permanent magnets (f_{PM}) and the MMF drop (f_{r0}) due to the flux passing through the iron ribs and the flux-barriers (flow-through flux along the d-axis). With proper machine design, the harmonic content of those two components can be minimized [4]. Thus, their contribution to eddy-current losses and to torque ripple will be disregarded here. In the following, the term f_{rs+} will be considered as the only component of the rotor MMF: $f_r = f_{rs+}$. The effects of such approximation will be discussed together with the results of the analysis (Section IV).

D. Air-Gap Flux Density Distribution

The air-gap flux density distribution is expressed by

$$B_g = \frac{\mu_0}{g} \cdot (f_s - f_r) \tag{13}$$

where g is the air-gap length and μ_0 is the magnetic permeability of free space.

E. Torque Ripple Expression With Stator Fundamental Harmonic Only

The torque ripple expression can be derived from the stator MMF and air-gap flux density expressions. According to the approach proposed in [10], the per-unit torque ripple can be expressed as

$$\frac{T_{ripple}}{T_1} = -\frac{1}{\sin\gamma_d} \sum_{\substack{k=6m\pm1 \\ m=1,2,3}} k \frac{\hat{f}_{sk}}{\hat{f}_{s1}} \frac{\hat{f}_{rk}}{\hat{f}_{r1}} \sin\left[(k \mp 1) \cdot \omega_r t \mp \gamma_d\right] \tag{14}$$

where T_1 is the average torque and the $\hat{f}_{rk}$ coefficients are constant because only the rotor MMF harmonics produced by the fundamental stator harmonic have been considered in the referenced paper. With reference to (11), $h = 1$ has been assumed and the considered rotor harmonic orders are $k = i \cdot n_r \pm 1$ only, while their argument $\varphi = (h-1) \cdot \omega_r t - \gamma_d$ is independent of time $(h - 1 = 0)$. The formula (14) represents the main ripple effect in many practical cases, but the disregarded rotor harmonic orders become significant in case $n_r > n_s$.

F. Extended Torque Ripple Expression

When $n_r > n_s$ (e.g., $n_s = 12$ with $n_r = 16$ or 20), the rotor reaction to stator harmonics higher than the fundamental one cannot be disregarded; in some cases, it can produce a significant component of the torque ripple. The per-unit ripple can be rewritten by (15), where the general expression of $\hat{f}_{rk}$(11) has been introduced into (14)

$$\frac{T_{ripple}}{T_1} = -\frac{1}{\sin\gamma_d} \cdot \sum_{i=0}^{\infty} \sum_{h=1}^{\infty} k \cdot \frac{\hat{f}_{sk}}{\hat{f}_{s1}} \frac{\hat{f}_{sh}}{\hat{f}_{r1}} \cdot \sin c\left(\frac{h\pi}{n_r}\right) \sin c\left(\frac{k\pi}{n_r}\right) \cdot \cos\left[(h \mp 1) \cdot \omega_r t \mp \gamma_d\right] \cdot \sin\left[(k \mp 1) \cdot \omega_r t \mp \gamma_d\right]. \tag{15}$$

The torque pulsation frequencies will be of the $(h \pm 1) \pm (k \pm 1)$ orders that are all multiples of six since $h \pm 1$ and $k \pm 1$, which appear in the arguments of cos( ) and sin( ) in (15), are always multiples of six. The simplified torque formula (14) can be obtained from (15) by posing $h = 1$.

G. Torque Ripple From Mirrored Harmonics

To put in evidence the ripple components disregarded in (14) and included in (15), the rotor harmonics of the type $k = h$ are considered here by posing $i = 0$ in (15). Such harmonics will be indicated in the following as "mirrored" rotor harmonics since they are the attenuated repetition of the hth stator harmonic in the rotor. For $k = h$, (15) becomes (16), where $\hat{f}_{r1} \cong \hat{f}_{s1}$ has been assumed

$$\frac{T_{\text{mirror}}}{T_1} \cong -\frac{1}{\sin\gamma_d} \cdot \sum_{h=1}^{\infty} h \cdot \left[\frac{\hat{f}_{sh}}{\hat{f}_{s1}} \cdot \sin c\left(\frac{h\pi}{n_r}\right)\right]^2 \cdot \frac{1}{2} \cdot \sin\left[2(h \mp 1)\omega_r t \mp 2\gamma_d\right]. \tag{16}$$

According to the argument of sin( ) in (16), the mirrored rotor harmonics $k = h$ produce a torque ripple at twice the frequency that would be intuitively related to the hth spatial order. Moreover, the factor one-half appears in (16). The mirror effect is significant with $n_r > n_s$ when the stator harmonics

are reproduced by the sampling filter of Fig. 2(b) with low attenuation.

To give an example of the mirror effect, a stator with $n_s = 12$ is considered, and the limit case $n_r \to \infty$ (distributed anisotropy, e.g., axially laminated rotor) is compared with the worst case ripple combination, that is, $n_r = 12$, as will be shown in Section III. The torque ripple produced by the combination of $h = 11$ and $k = 11$ is evaluated in both cases since $h = 11$ and $h = 13$ are the stator slot-harmonic orders that mostly contribute to torque ripple [10]. From $n_r \to \infty$, it follows that $\mathrm{sinc}(h\pi/n_r) \to 1$; thus, $\hat{f}_{r11} = \hat{f}_{s11}$ from (9) and (11). Note that $\hat{f}_{s11}/\hat{f}_{s1} = 1/11$; hence, the component $h = 11$ of (16) results in a per-unit torque ripple with an amplitude of nearly $(1/\sin\gamma_d)(11/2) \cdot (1/11)^2 = (1/22/\sin\gamma_d)$ and an argument pulsating at 24 ω_r (twice the stator slot order). Dealing with $n_r = 12$, the stator fundamental MMF $(h = 1)$ produces the rotor slot order $k = 11$. Applying (14) with $k = 11$, or equivalently, (15) with $h = 1$, $i = 1$, and $k = 11$, leads to a torque ripple component with an amplitude near to $(1/11/\sin\gamma_d)$ (twice the amplitude found with the axially laminated rotor) and an argument pulsating at 12 ω_r. The same conclusions come out for $k = 13$, that is, the other stator slot-harmonic order. Thus, the mirror effect is capable of producing torque ripple components with an amplitude up to 50% of the worst case ripple components considered in the literature. For finite values of n_r, the mirror effect is reduced because the rotor does not exactly copy the hth stator harmonic. In practical cases, the mirror effect is significant when $n_r > n_s$, while for $n_r < n_s$, this effect vanishes due to $\mathrm{sinc}^2()$ attenuation. Of course, for $n_r > n_s$, the mirror effect is lower when n_r is near n_s, but the combinations $n_r = n_s$ and $n_r = n_s \pm 2$ must be always avoided, as shown in [10] and confirmed in the following.

H. Iron Loss Formulation

The eddy-current losses will only be considered in the proposed approach. The approximation is valid for the high speed losses of IPM machines [8] and is also confirmed by FEA. The iron losses are calculated separately in the stator teeth (t), stator yoke (y), and rotor channels (r) along flux paths where the flux density distribution may be assumed to be constant. The loss terms concentrated around the air-gap surface, both on the stator and rotor surfaces are not modeled here. Additional comments will be given in Section IV.

The air-gap flux density can be derived according to (13), where the considered f_s wave (3) is a staircase function that includes all the stator MMF harmonic content (slot and belt harmonics). The flux density in the jth stator tooth is expressed in (17) as the average of the air-gap flux density over one tooth pitch

$$B_{t,j}(\vartheta) = \frac{1}{b_t \Delta_s} \int_{\alpha_{j-1}}^{\alpha_j} B_g(\alpha, \vartheta) \cdot d\alpha \tag{17}$$

where $j = 1 \div n_s$. The parameter $b_t (< 1)$ is the ratio between the stator tooth width and the stator tooth pitch at the air gap.

The flux density in the stator yoke (18) follows accordingly

$$B_y(\vartheta) = \frac{1}{2} \cdot \sum_{j=1}^{1/2\, n_s} B_{t,j}(\vartheta). \tag{18}$$

Only the even values of n_s have been considered in (18). A similar expression, however, can be found for odd numbers. The flux density in the kth rotor channel $(B_{r,k})$ is the average of the air-gap flux density over one rotor pitch

$$B_{r,k}(\vartheta) = \frac{1}{\Delta} \int_{\xi_{k-1}}^{\xi_k} \frac{B_g(\xi, \vartheta)}{b_{r,k}} \cdot d\xi \tag{19}$$

where $k = 1 \div n_{ch}$ and $n_{ch} = \mathrm{floor}(n_r/4) + 1$ are the number of rotor channels of one pole and the parameter $b_{r,k} (< 1)$ is the ratio between the kth rotor channel width and the rotor pitch at the air gap.

The eddy-current loss per volume for a nonsinusoidal waveform is expressed by

$$p_{\mathrm{eddy}} = \frac{\sigma \cdot d^2}{12} \cdot \frac{\omega^2}{2\pi} \cdot \int_0^{2\pi} \left(\frac{\partial B}{\partial \vartheta} \right)^2 d\vartheta \tag{20}$$

where σ is the electrical conductivity, d is the steel lamination thickness, and steady-state electrical speed ω is assumed. The loss model can be expressed as in

$$P_{\mathrm{eddy}} = p_{\mathrm{eddy},t} \cdot V_t + p_{\mathrm{eddy},y} \cdot V_y + \sum_{k=1}^{n_{ch}} (p_{\mathrm{eddy},rk} \cdot V_{rk}) \tag{21}$$

where V_t, V_y, and $V_{r,k}$ are the volumes of the stator teeth, the stator yoke, and the kth rotor channel, respectively. The sharing of the machine volume among the three terms V_t, V_y, and V_r depends on the machine geometry and is summarized by a small set of parameters (bore to outer diameter, rated air-gap flux density, pole pairs). As a first approximation, n_s and n_r do not affect the volume sharing.

III. Application of the Proposed Method

The model described in Section II has been implemented in Matlab for a series of IPM motors with different n_s, n_r combinations. All the motors have a common geometry (stator dimensions, rotor outer and inner diameters, number of poles, number of turns) and a common performance target in terms of rated torque, voltage, current, and operating speed range. The number of examples is wide and permits to draw some general conclusions about the design tradeoffs between losses and torque ripple. The FEA validation is given for the most significant cases, most of which are with $n_s = 12$ mainly because low numbers produce significant torque ripple. The correspondence with the FEA results is satisfactory; thus, the model can be considered as a tool to compare different design choices.

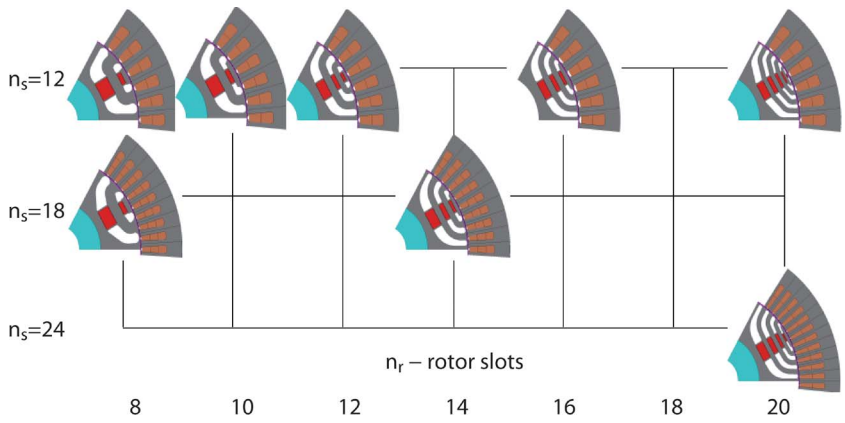

Fig. 4. Example machines designed for FEA validation.

A. Terms of Comparison

As said, the example machines have been designed with the same specifications. In particular, the same short-circuit current (or characteristic current) has been pursued in the design of all the machines as it is representative of the operating region at high speed [8], and it is assumed that the characteristic current coincides with the rated current for all the motors. For these reasons:

- the short-circuit condition at maximum operating speed will be the one considered for eddy-current loss calculation ($i_d = i_{cc}, i_q = 0$); and
- the same current amplitude and phase angle conditions are adopted for all the machines for torque ripple evaluation. The setpoint $|i| = i_{cc}$, $\gamma_d = 153.4^\circ$ (that is, $i_d = -2 \cdot i_q$) is chosen since it is representative, with good approximation, of the maximum torque angle at rated current for all the designed machines.

Dealing with point 1, in short-circuit condition, the disregarded MMF terms (f_{PM}, f_{r0}) compensate each other (at least the fundamental components), and this partially confirms the significance of the adopted approximation. Dealing with point 2, the obtained torque is not exactly the same for all the machines; thus. the torque ripple comparison will be given in per-units of the average torque (T_1) of each one. Also, in this case, the disregarded terms (f_{PM}, f_{r0}) tend to compensate each other. In any case, under the assumed design hypotheses, they mainly contribute to the average torque and very few to the ripple; hence, they introduce an error in terms of per-unit ripple that is small and more or less the same for all the considered machines.

The considered stator slot values are $n_s = 12, 18, 24$ associated with n_r that varies from 8 to 20. As said, the model will be applied to all the machines, while the FEA validation will be given only for the most significant ones. In Fig. 4, the set of the FEA-simulated machines is reported, ordered per slot numbers. The torque ripple summary will be presented first, followed by the analogous summary of iron losses.

B. Torque Ripple

The peak torque ripple is represented in per-units of the average torque of each motor. The results of the model are shown in Fig. 5 and the FEA results are reported in Fig. 6 for comparison. As expected, the worst case is with $n_r = n_s$, followed by the side values $n_r = n_s \pm 2$ (e.g., 12/10, 12/14, 18/16, 18/20 in Fig. 5). A second consideration is that a higher n_s number is, in general, beneficial for the torque ripple because the stator MMF harmonic content is reduced in this case. Last,

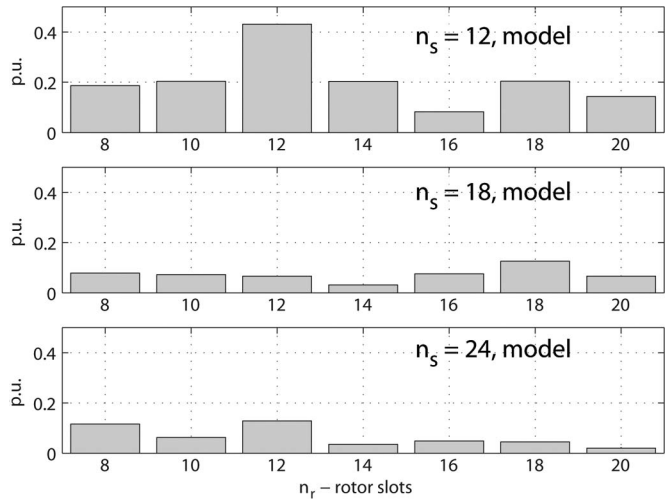

Fig. 5. Per-unit torque ripple—model.

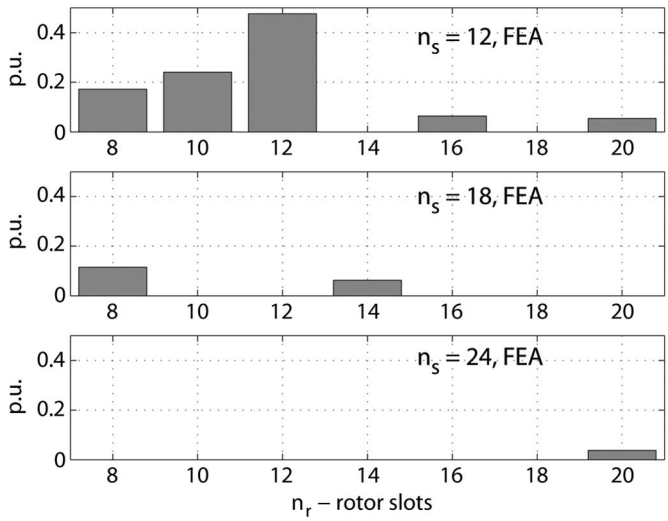

Fig. 6. Per-unit torque ripple—FEA.

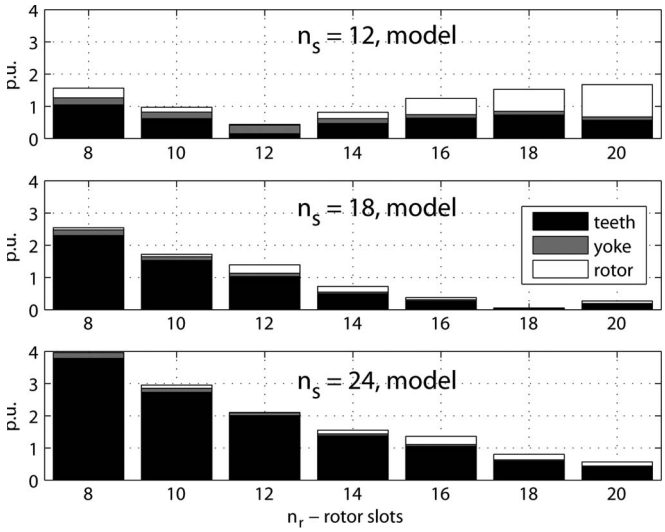

Fig. 7. Per-unit losses—model.

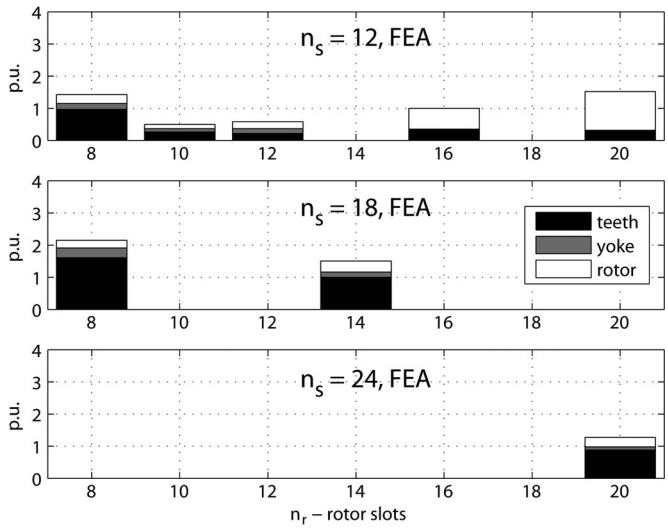

Fig. 8. Per-unit losses—FEA.

when n_s and n_r are far from each other, the ripple tends to rise again. According to Fig. 5, the best ripple combinations for the considered $\mathrm{n_s}$ values are 12/16, 18/14, and 24/20, respectively. All the favorable combinations have in common $|n_s - n_r| = 4$ [4]. With odd n_s values, different combinations can be found [10]. However, odd n_s numbers have not been included in the proposed examples to not complicate the proposed analysis further.

C. Eddy-Current Losses

The harmonic losses calculated by the model for all the machines are shown in Fig. 7. The first conclusion that can be drawn is that $n_s = n_r$ is the best solution for high speed harmonic losses, and that the total loss (stator + rotor) rises progressively as the distance between n_r and n_s increases. In particular, for $n_r < n_s$, the stator losses prevail while the rotor losses prevail for $n_r > n_s$. This is in agreement with the results obtained in [7], [9]. Nevertheless, as for torque ripple, the eddy-current losses tend to reduce as n_s is increased, at least where n_r is around n_s (Fig. 7), but not when n_s and n_r are far from each other. Last, the yoke losses are significant only in the case $n_r = n_s$, even if the scale of Fig. 7 does not permit to distinguish the case 18/18. The same base value (2 800 W) has been used for all the diagrams of Figs. 7 and 8, where the FEA results are given. Such value represents the total losses of the 12/16 machine according to the FEA.

D. Design Tradeoffs

With $n_s = 12$, the best solution appears to be $n_r = 16$, which is as near as possible to 12 $(n_s + 4)$ and has a low ripple. The complementary solution $n_r = 8$ $(n_s - 4)$ has similar losses, but much more ripple (see Figs. 11 and 12). The only concern about the choice of $n_r > n_s$ is that the rotor losses are high in this case. With standard machines (inner rotor) and standard cooling solutions, this can overheat the rotor (PM, bearings), particularly for machines with very high speed ranges. With $n_s = 18$ and $n_s = 24$, better combinations are possible. In particular,

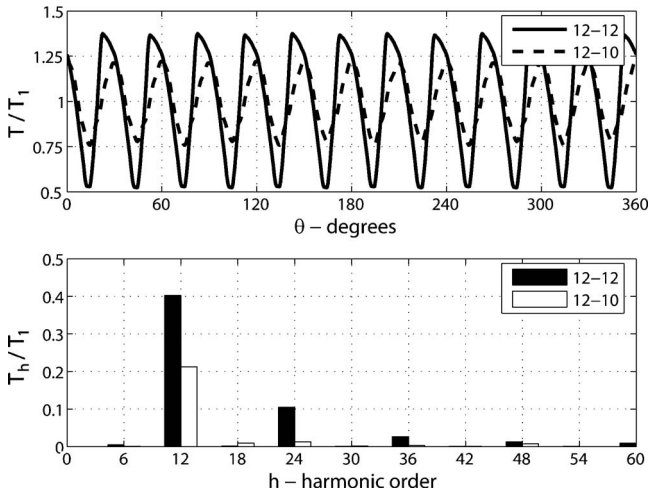

Fig. 9. FEA-calculated per-unit torque ripple of the combinations $ns = 12$, $nr = 12$ and 10.

the $n_r = n_s - 4$ solutions are chosen in those cases for their low ripple and reduced losses, which are mainly localized on the stator. The suggested design tradeoffs are 18/14 and 24/20, respectively.

IV. Detailed FEA Results and Experimental Validation

Some significant examples of torque ripple waveforms are presented in order to discuss their harmonic content according to the proposed formula (15). Additional comments are given about how the losses have been FEA-calculated and which terms have been considered or disregarded.

A. n_s, n_r Combinations With Common Slot Harmonic Orders

As previously mentioned, the combinations $n_r = n_s$ and $n_r = n_s \pm 2$ must be avoided because they present common slot harmonic orders. Two examples are shown in Fig. 9, where $n_r = 10$ and 12 are associated to a $n_s = 12$ stator. In the 12/12 case, the slot harmonics combine to give a 12th order ripple and

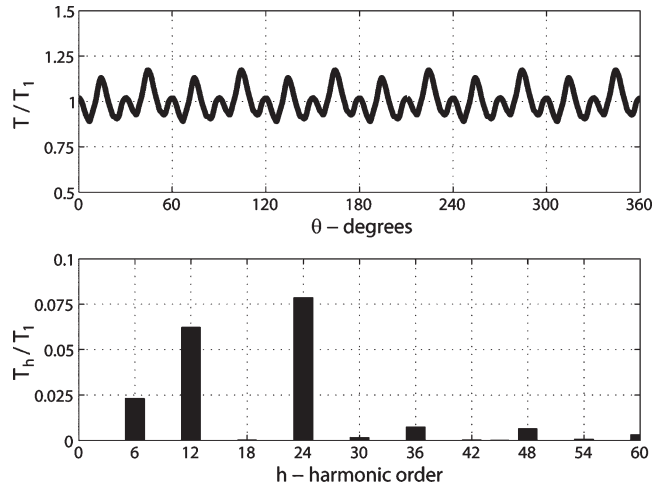

Fig. 10. FEA-calculated per-unit torque ripple for $ns = 12$, $nr = 8$.

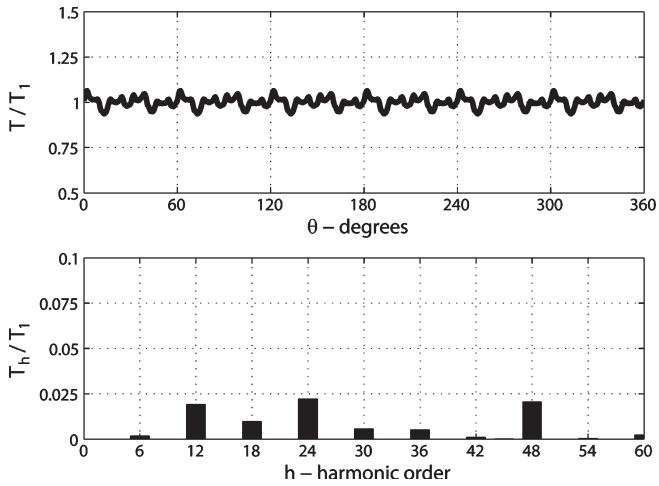

Fig. 11. FEA-calculated $ns = 12$, $nr = 16$, per-unit torque ripple.

all its multiple orders (24, 36, ...). In the 12/10 case, the slot order 11 is common to the stator and the rotor and produces the 12th order component T_{12}. The multiples of slot harmonics do not match in this case. The ripple of the 12/10 case is nearly one-half of that of 12/12 according to Fig. 9.

The 12/8 case shown in Fig. 10 is representative of slot combinations with low minimum common multiples. In this case, the slot orders do not combine directly; still, their multiples (23 and 25) do as the significant T_{24} component stands for T_6 and T_{12} are generated by the belt harmonics, as will be explained in the next examples.

B. Mirror Effect for $n_r > n_s$

When inconvenient design choices like 12/12 or 12/10 are avoided, the torque ripple drops significantly, as shown in Fig. 11 for the case 12/16. The mirror effect represents a significant part of the torque ripple (T_{24}, in particular). Table I shows how to interpret the torque ripple formula presented in (15) since in the 12/16 case harmonic interactions of all the kinds can be found. In Table I, the stator slot harmonics (h) are represented along the horizontal axis. Each h order produces on the rotor a mirror term $(k = h)$ and infinite sideband terms.

TABLE I
STATOR AND ROTOR MMF HARMONICS FOR $ns = 12$, $nr = 16$

f_s	h	1	5	7	11	13
f_r	k = h	1	5 T_{12}	7 T_{12}	11 T_{24}	13 T_{24}
	k = 16 – h	15	11 T_6,T_{18}	9	5 T_6,T_{18}	3
	k = 16 + h	17 T_{18}	21	23	27	29

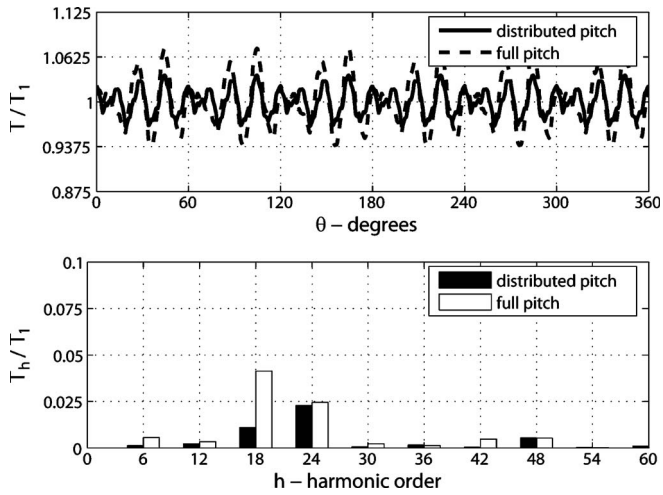

Fig. 12. FEA-calculated per-unit torque ripple for ns = 24, nr = 20.

Only the first sideband pair is considered here $(16 \pm h)$. The shaded terms are multiples of 3 and do not produce torque. The mirror effect is produced both by the stator slot harmonics $(h = 11, 13)$, which give a T_{24} component, and by the stator belt harmonics $(h = 5, 7)$, which produce a T_{12} component. The interaction of $k = 5$ (sideband of h = 11) with $h = 5$ produces two components T_6 and T_{18} according to (15). Note that the ripple order is $(h \pm 1) \pm (k \pm 1)$. Similarly, the interaction of $k = 11$ (sideband of $h = 5$) with $h = 11$ produces two other components T_6 and T_{18} that can magnify or attenuate the former ones according to the phase relationship given in (15). In Fig. 11, the total T_6 is small (the two contributions of $h = 5$ and $h = 11$ are out of phase), while T_{18} is bigger (the two contributions are in phase). However, different results may be found with different current angles γ_d according to (15).

C. No Mirror With $n_r < n_s$ and Effect of Belt Harmonics

The combination 24/20 shown in Fig. 12 leads to very low ripple. In this case, the stator slot harmonics $(h = 23, 25)$ are badly "mirrored" by the rotor and a low T_{48} results. Reduced-pitch winding and full-pitched winding are shown in Fig. 12 to underline the impact of stator belt harmonics, which produce the T_{18} component.

D. Limitations of the Proposed Model

The combination 18/14 in Fig. 13 has been chosen to underline the limits of the proposed model. All the ripple harmonics are eliminated except for T_{18}, which is not justified by (15). The cause of such a ripple component may rely in the rotor MMF

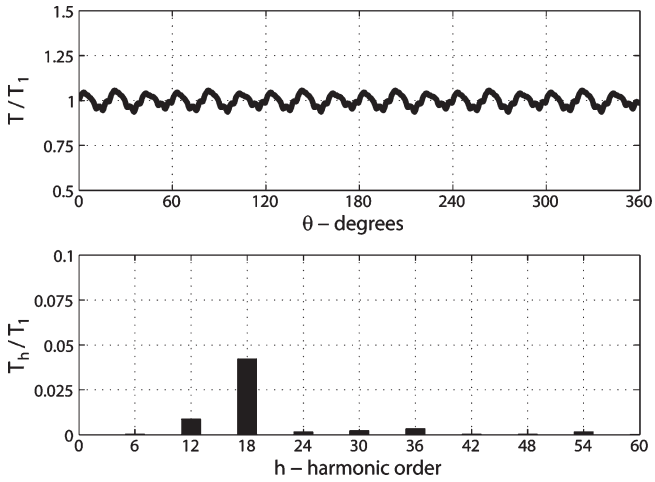

Fig. 13. FEA-calculated per-unit torque ripple for ns = 18, nr = 14.

harmonic content, where the contribution of the f_{PM} and f_{r0} terms was excluded due to the accurate rotor design. Despite the effort put in the design of the rotor geometry, residual $k = 17, 19$ components could not be excluded and this may justify the 4% ripple that appears in Fig. 13.

E. Experimental Validation of the Finite-Element Analysis

The results obtained by the FEA are compared with experimental results for a 12/16 machine. The prototype from which the example machines of Fig. 4 have been derived is a 12/16 machine. Its torque ripple, calculated with FEA, is shown in Fig. 11. Unfortunately, the stator of such machine is skewed by one stator slot pitch and the resulting torque ripple is not significant. Another 12/16 prototype, designed for home appliances, has been tested and the measured torque has been compared with the FEA-calculated one in Fig. 14. The motor is driven at constant speed (10 rpm) by a speed-controlled drive with a very high ratio-reducing gear. The IPM motor under test is current-controlled ($i_d = -3$ A, $i_q = 1.5$ A, according to Section III-A) and the torque is measured by means of a torque meter. The mean value of the measured torque is 1.7 Nm while the calculated one (2D FEA) is 1.5 Nm. Such discrepancy could be due to the end-effects that are significant in such motor and are not taken into account by the 2D FEA model. Nevertheless, the per-unit ripples are very similar in Fig. 14, as well as the torque spectra.

Dealing with high speed core losses, the experimental validation of FEA is more difficult since it would require that a series of motors with the same frame and different slot combinations, including "bad design" combinations, be actually designed. In future works, three IPM motor prototypes designed for traction with similar sizes and operating speeds will be compared, and the criteria for normalizing the high speed losses of machines with different sizes, speeds, and steel grades will be also introduced.

F. FEA Calculation of Eddy-Current Losses

A comprehensive model of iron losses, valid for nonsinusoidal flux density waveforms including alternating and rotational components [3], [5], [6] has been adopted for the FEA validation of the proposed analysis. The iron losses are calculated from the field solution of a transient with motion FEA simulation: the stator and rotor flux density distribution is downloaded from the FEA solution and the loss model is applied to each triangle of the 2D mesh. The iron loss processing tool has been purposely developed in Matlab and the steel loss data are taken from datasheets [12]. As said, in the analytical model (21) and in the literature, the losses are calculated along those steel paths where the flux density is uniformly distributed. In other words, the model does not include loss terms like the one concentrated around the air-gap surface, as shown in Fig. 15(b). Surface losses can give a significant contribution to total losses and such contributions are not the same for all the considered machines, but they are very similar for those machines with the same stator slots; thus, the presented results remain reasonably valid.

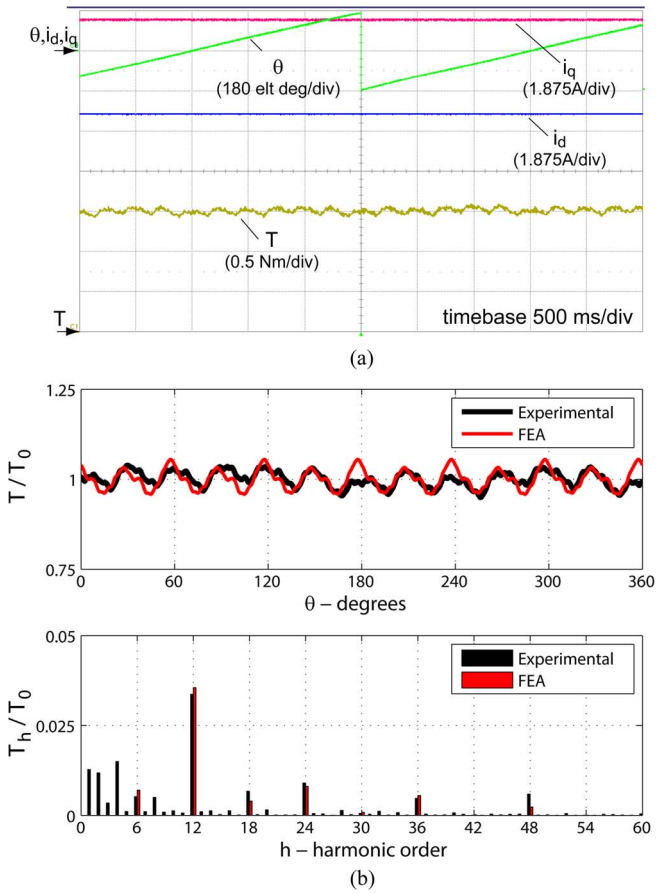

Fig. 14. Torque measurement for a $n_s = 12$, $n_r = 16$ motor with 2 pole-pairs. The prototype is purposely nonskewed. It is designed for home appliances and it is different from the machine considered in Figs. 11 and 15. (a) Test conditions are $i_d = -3.0$ A, $i_q = 1.5$ A, and 10 rpm. (b) Comparison between measured and FEA-calculated torque ripple.

V. Conclusion

This paper has dealt with the optimal combination of stator and rotor slots for IPM motors with wide constant-power speed range. A tradeoff between minimal losses at high speed and

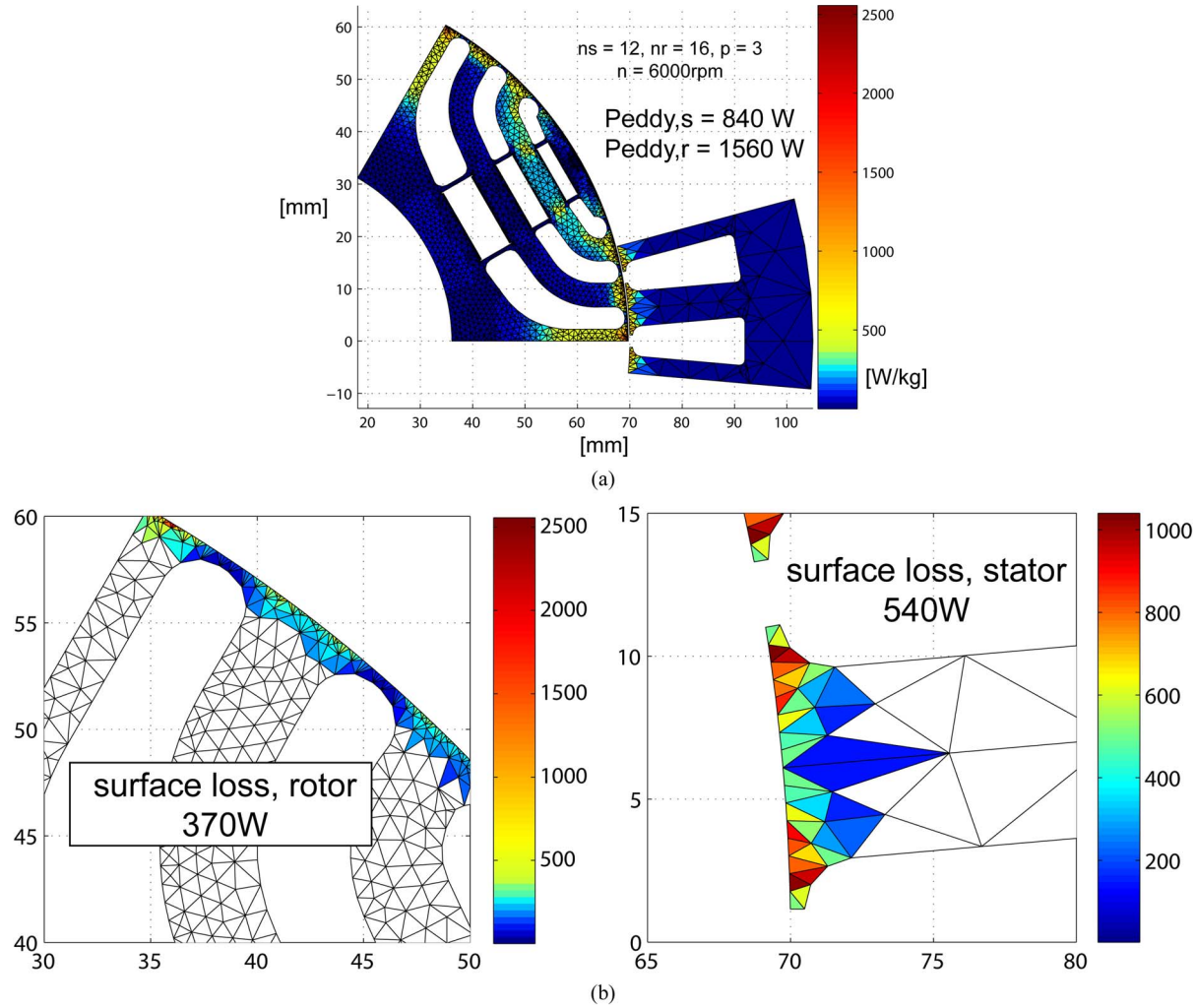

Fig. 15. FEA-calculated losses, example case 12/16. (a) Map of the specific loss (W/kg). (b) Detail of the surface losses.

minimal torque ripple is pursued in a general manner based on a simplified model. An analytical expression of the torque ripple has been presented based on the Fourier expansions of the MMF stator and rotor waves. The torque ripple model is confirmed by several FEA simulations and by one experimental test. Based on the model results over a number of example machines, the criteria for selecting the best compromise motor are given. In general, the number of stator and rotor slots should not be too near (for torque ripple) and neither too far (for core losses). A larger number of stator slots with respect to rotor slots could be preferred, because this produces less core losses in the rotor than in the stator. The same procedure could be repeated with different specifications according to the requirements of the single application.

REFERENCES

[1] R. Schifer and T. A. Lipo, "Core loss in buried magnet permanent magnet synchronous motors," *IEEE Trans. Energy Convers.*, vol. 4, no. 2, pp. 279–284, Jun. 1989.

[2] V. Zivotic-Kukolj, W. L. Soong, and N. Ertugrul, "Iron loss reduction in an interior PM automotive alternator," *IEEE Trans. Ind. Appl.*, vol. 42, no. 6, pp. 1478–1486, Nov./Dec. 2006.

[3] B. Stumberger, A. Hamler, and B. Hribernik, "Analysis of iron loss in interior permanent magnet synchronous motor over a wide-speed range of constant output power operation," *IEEE Trans. Magn.*, vol. 36, no. 4, pp. 1846–1849, Jul. 2000.

[4] A. Vagati, M. Pastorelli, G. Francheschini, and S. C. Petrache, "Design of low-torque-ripple synchronous reluctance motors," *IEEE Trans. Ind. Appl.*, vol. 34, no. 4, pp. 758–765, Jul./Aug. 1998.

[5] F. Fiorillo and A. Novikov, "An improved approach to power losses in magnetic laminations under nonsinusoidal induction waveform," *IEEE Trans. Magn.*, vol. 26, no. 5, pp. 2904–2910, Sep. 1990.

[6] J. G. Zhu and V. S. Ramsden, "Improved formulations for rotational core losses in rotating electrical machines," *IEEE Trans. Magn.*, vol. 34, no. 4, pp. 2234–2242, Jul. 1998.

[7] S.-H. Han, T. M. Jahns, and Z. Q. Zhu, "Analysis of rotor core eddy-current losses in interior permanent magnet synchronous machines," in *Conf. Rec. IEEE IAS Annu. Meeting*, Oct. 5–9, 2008, pp. 1–8.

[8] S.-H. Han, T. M. Jahns, and Z. Q. Zhu, "Design tradeoffs between stator core loss and torque ripple in IPM machines," in *Conf. Rec. IEEE IAS Annu. Meeting*, Oct. 5–9, 2008, pp. 1–8.

[9] S.-H. Han, W. L. Soong, and T. M. Jahns, "An analytical design approach for reducing stator iron losses in interior PM synchronous machines during flux-weakening operation," in *Conf. Rec. 42nd IEEE IAS Annu. Meeting*, Sep. 23–27, 2007, pp. 103–110.

[10] T. M. Jahns and W. L. Soong, "Torque ripple reduction in interior permanent magnet synchronous machines using the principle of mutual harmonics exclusion," in *Conf. Rec. 42nd IEEE IAS Annu. Meeting*, Sep. 23–27, 2007, pp. 558–565.

[11] R. Isermann, *Digital Control Systems*. New York: Springer-Verlag, 1981.

[12] S. Sprague, "Lamination steels, third edition," in *The Lamination Steels Research Project*. South Dartmouth, MA: EMERF, 2007.

Gianmario Pellegrino (M'06) received the M.Sc. and Ph.D. degrees in electrical engineering from the Politecnico di Torino, Turin, Italy, in 1998 and 2002, respectively.

Since 2002, he has been with the Department of Electrical Engineering, Politecnico di Torino, first as a Research Associate and currently as an Assistant Professor teaching courses on power electronics and electric drives. He is involved in research projects for the public sector and for private groups. He has authored more than 30 technical papers and is the holder of one international patent. His field of interest is electric drives, particularly in motor design and digital control. He works in the fields of electric traction and design of direct-drive generators for wind energy production. He was a Guest Researcher at Aalborg University, Denmark, in 2002.

Paolo Guglielmi (M'07) was born in Imperia, Italy, in 1970. He received the M.Sc. degree in electronic engineering and the Ph.D. degree in electrical engineering from the Politecnico di Torino, Turin, Italy, in 1996 and 2001, respectively.

In 1997, he joined the Department of Electrical Engineering, Politecnico di Torino, where he became a Researcher in 2002. He has authored several papers published in technical journals and conference proceedings. His fields of interest include power electronics, high-performance drives, and computer-aided design of electrical machines.

Dr. Guglielmi is a Registered Professional Engineer in Italy.

Alfredo Vagati (M'88–SM'92–F'98) received the Laurea degree in electrical engineering from the Politecnico di Torino, Turin, Italy, in 1970.

After a few years working in industry with Olivetti, he joined the Politecnico di Torino in 1975 as Assistant Professor. In 1990, he became Professor of Electrical Machines and Drives at the University of Cagliari, Cagliari, Italy. In 1991, he rejoined the Politecnico di Torino in the same capacity. His scientific activity in the field of electrical machines and drives has focused mainly on high-performance ac drives. He has been involved in several industrial projects in the field of ac drives as both a designer and a scientific reference. His most important activity is the design and control of newly developed, high-performance synchronous reluctance motors. He has led several countrywide and European research projects in the field of design and control of synchronous-machine-based drives for different applications, including home appliances and the automotive world. He has authored or coauthored more than 100 technical papers.

Prof. Vagati is a permanent member of the Technical Program Committee of the PCIM International Conference and Exhibition.

Franco Villata received the Laurea degree in electrical engineering from the Politecnico di Torino, Turin, Italy, in 1965.

From 1965 to 1966, he was with the Politecnico di Torino as an Assistant Professor. From 1966 to 1967, he was with ENEL, working in power plant design. He rejoined the Politecnico di Torino as an Assistant Professor in 1967. From 1983 to 1986, he was an Associate Professor and, in 1986, he became a Professor of Electrical Machines and Drives at the Politecnico di Torino. He retired in 2008, but still actively contributes to the research activity of a working group. His research interests concern electrical machines and power electronics.